PERGAMON

Available online at www.sciencedirect.com

SCIENCE DIRECT®

Electrochimica Acta 48 (2003) 1395–1401

ELECTROCHIMICA Acta

www.elsevier.com/locate/electacta

Corrosion study of surface-modified vanadium-free titanium alloys

M.F. López [a,*], J.A. Jiménez [b], A. Gutiérrez [c]

[a] *Instituto de Ciencia de Materiales de Madrid, CSIC, Departamento de Fisica e Ingenieria superficies, Cantoblanco, E-28049 Madrid, Spain*
[b] *Centro Nacional de Investigaciones Metalúrgicas, CSIC, Avda. Gregorio del Amo 8, E-28040 Madrid, Spain*
[c] *Departamento de Física Aplicada, Universidad Autónoma de Madrid, Cantoblanco, E-28049 Madrid, Spain*

Received 12 December 2002; received in revised form 12 December 2002

Abstract

The present work is part of an investigation aimed to improve the corrosion resistance of three vanadium-free titanium alloys of biomedical interest, Ti–6Al–7Nb, Ti–13Nb–13Zr and Ti–15Zr–4Nb, by growing on their surfaces an oxide protective layer. For this goal, different samples were oxidized in air at 750 °C for times ranging from 6 to 48 h. Thickness, morphology and composition of the oxide scales for different oxidation times were investigated by using scanning electron microscopy (SEM) and X-ray diffraction (XRD). After equal oxidation time, the Ti–6Al–7Nb alloy exhibited a thinner, more compact and dense oxide layer than the TiNbZr alloys, indicating a slower oxidation rate. Several oxidation times were used in order to obtain oxide scales with similar properties for the three alloys. Different electrochemical techniques were then applied to evaluate the corrosion behavior of the different samples. The oxidized Ti–6Al–7Nb alloy showed the lowest corrosion current densities as well as the best pitting corrosion behavior, and is thereby considered as the best of these materials for biomedical applications.

Keywords: Titanium alloys; Electrochemical techniques; Corrosion; Oxidation; Biomaterials

1. Introduction

Their excellent mechanical properties combined with a satisfactory corrosion behavior make titanium and its alloys materials widely used for biomedical applications [1–3]. However, although conventional metallic biomaterials exhibit high corrosion resistance values, the material degradation of a metal is never negligible [4,5]. The corrosion process is determined by the ion release of metallic species and is, therefore, mainly a surface phenomenon. For titanium base alloys, the high titanium content promotes an easy reaction with oxygen from atmosphere due to its strong affinity for oxygen [6]. Thus, these materials show a tendency to form a stable and tightly adherent protective oxide layer on their surfaces. This layer provides protection against the harmful effects of aggressive environments and is the responsible of the good corrosion behavior of these materials.

In order to improve not only the corrosion behavior of metallic biomaterials but also their biocompatibility and mechanical properties, numerous surface modification treatments have been studied [7–14]. A simple method to generate a barrier on the alloy surface is to treat it thermally in an oxygen rich atmosphere, which produces a surface oxide layer. This method has already been investigated with different biomaterials as well as with candidates to biomaterials [14–16]. In biomedical applications, the chemical composition and stability of the surface oxide layer is of high interest because the surface of biomaterials is in direct contact with biological tissues.

During the last 50 years in which titanium has been commercially available, many titanium alloys have been developed. However, Ti–6Al–4V has accounted for about 50% of the total market and has, thus, become a standard alloy. For this reason, Ti–6Al–4V has been the first titanium alloy used in prosthetic applications. Recently, vanadium has been classified as one of the elements of the toxic group [17]. The possibility of V release and the increasing trend in the use of prostheses have encouraged the development of new alloys without

* Corresponding author. Tel.: +34-913-34-9000; fax: +34-913-72-0623.

0013-4686/03/$ - see front matter
doi:10.1016/S0013-4686(03)00006-9

V for use in biomedical devices, such as Ti–6Al–7Nb, Ti–15Mo–3Nb, Ti–13Nb–13Zr and Ti–15Zr–4Nb [17–19].

To determine the suitability of a material for body implant applications, several properties must be evaluated. Amongst these properties, the corrosion behavior is of crucial interest, because the ion release from the implant to the surrounding tissues may give rise to biocompatibility problems. The objective of this work is to determine the corrosion behavior of three different titanium alloys, Ti–6Al–7Nb, Ti–13Nb–13Zr and Ti–15Zr–4Nb, after an oxidation treatment at 750 °C with the aim of determining the protective capacity of the oxide films formed on the alloys during the oxidation process. To achieve this objective different electrochemical techniques were applied. The electrochemical impedance spectroscopy (EIS) and the linear polarization method were used to evaluate the uniform corrosion process. Additionally, since it is very important for a biomaterial to obtain information about the probability of localized loss of passivity, anodic polarization curves were recorded to asses the pitting corrosion resistance of the samples.

2. Experimental

Three titanium alloys with compositions (in weight%) Ti–6Al–7Nb, Ti–13Nb–13Zr and Ti–15Zr–4Nb have been prepared by arc melting and then casting in a copper coquille under high vacuum. Oxidation tests were carried out on specimens cut from as-cast ingots by electrospark erosion. Before the oxidation process, the major sample surfaces were abraded and polished using diamond pastes with successively smaller particle size. In the final stage of this process, colloidal silica was used to ensure a surface free of mechanical deformation. Finally, the samples were ultrasonically cleaned with acetone before oxidation. Oxidation was carried out in air in a tube furnace at 750 °C for exposition times of 6, 24 and 48 h.

Characterization of oxidation products was performed using various techniques. The different phases present in the oxide scale were identified from the X-ray diffraction (XRD) patterns obtained employing Cu K_α radiation. The cross sections of the oxidized samples were examined by scanning electron microscopy (SEM). To prevent scale loss during metallographic preparation, the surface of the oxidized samples were coated with a thin gold layer by sputtering and then a thicker layer of copper was electrolytically deposited.

Corrosion behavior of the oxidized Ti alloys was evaluated at 37 °C using as electrolyte an aerated solution, the Hank's solution, which simulates the physiological media of the human body. This solution, with pH 7.4, has the following chemical composition: 8 g l^{-1} NaCl, 1 g l^{-1} glucose, 0.4 g l^{-1} KCl, 0.35 g l^{-1} $NaHCO_3$, 0.14 g l^{-1} $CaCl_2$, 0.1 g l^{-1} $MgCl_2 \cdot 6H_2O$, 0.06 g l^{-1} $Na_2HPO_4 \cdot 2H_2O$, 0.06 g l^{-1} KH_2PO_4 and 0.06 g l^{-1} $MgSO_4 \cdot 7H_2O$. A saturated calomel electrode was used as a reference electrode and a platinum wire as counter electrode. The surface area of the sample, i.e. the working electrode, exposed to the electrolyte was flat with a circular shape of about 25 mm^2. The electrochemical experiments were conducted on four different specimens for each alloy and oxidation temperature. The following electrochemical techniques were performed to determine the corrosion properties of the oxidized titanium alloys:

- EIS. To use this method, a sinusoidal potential signal of 10 mV amplitude was applied within a frequency range from 0.001 to 64000 Hz, and the resulting current was measured. Data were recorded at 5-frequencies/decade.
- Determination of the anodic polarization resistance, R_p, by means of the linear polarization method using a potentiostatic step. The sample/electrolyte system can be altered by applying a potential step, ΔE, for example of 10 mV. The response of this system to ΔE is an intensity flow, ΔI, that is registered versus time up to 60 s. The polarization resistance value is deduced from the equation $R_p = \Delta E/\Delta I$.
- Anodic polarization potentiodynamic curves to evaluate the susceptibility to the pitting corrosion at a scan rate of 0.16 mV s^{-1}. These experiments were conducted after 18 days of immersion in Hank's solution, i.e. at the end of the other complementary electrochemical techniques, because it can probably generate the break of the outer layer. The fundamental classical parameters upon which the interpretation of the susceptibility to pitting corrosion are based are the following:
  - The corrosion potential, E_{corr}, that corresponds to the system sample/electrolyte without any external perturbation.
  - The breakdown potential, E_b, that corresponds to the local break of the passive layer. At this point, the intensity grows significantly, due to the pitting formation.
  - The protection or repassivation potential that is reached when the formed pits stop their propagation.

It is important to notice that between the corrosion potential, E_{corr}, and the breakdown potential, E_b, a passive material maintains its passive state, undergoing localized corrosion at $E > E_b$, with the formation of pits.

Since this work is part of an extensive study aimed to investigate these three Ti alloys for biomedical applications, the corrosion behavior of these materials without

thermal treatment, i.e. in as-received state, have been already evaluated in previous works. Thus, the results of the electrochemical tests for the control specimens (the alloys in as-received state) are detailed elsewhere [20].

3. Results and discussion

Cross-sectional views of the Ti–6Al–7Nb, Ti–13Nb–13Zr and Ti–15Zr–4Nb alloys samples oxidized for 24 h at 750 °C are shown in Fig. 1. These SEM micrographs show clear differences in the thickness of the oxide scales formed on the three alloys. The Ti–6Al–7Nb alloy developed a thin and homogeneous scale of about 2 μm in size, whereas the TiNbZr alloys present a thicker scale, of around 10 and 25 μm for Ti–13Nb–13Zr and Ti–15Zr–4Nb, respectively. The upper regions of the micrographs shown in Fig. 1 correspond to the coarse microstructure with two phases of the metallic materials. These microstructures are rather similar to that of the same alloys without thermal treatment, which were showed and discussed in previous studies performed on these alloys in the as-received condition [20].

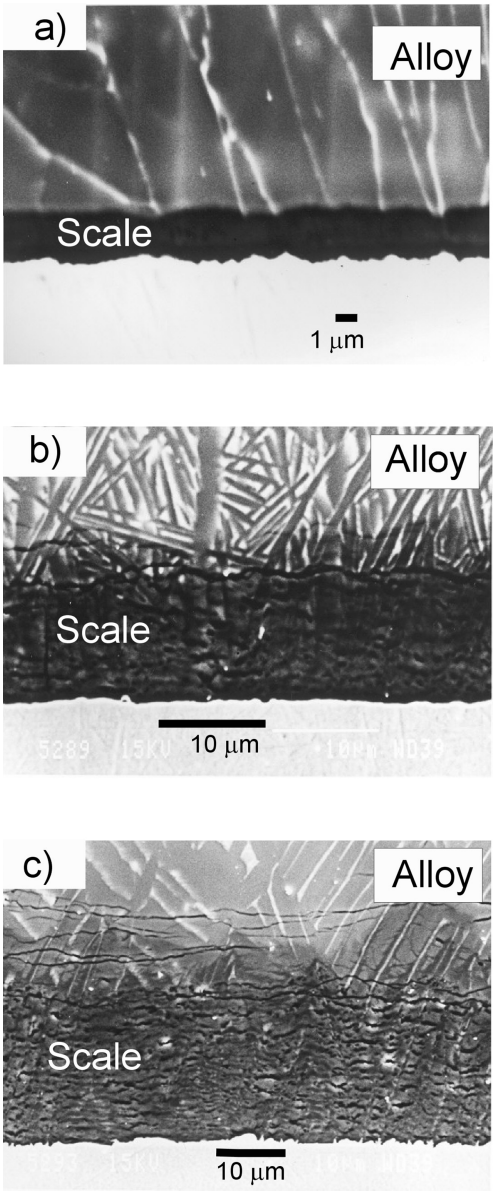

Fig. 1. Cross-sectional SEM micrograph of the oxide scale formed after an oxidation treatment at 750 °C for 24 h on (a) Ti–6Al–7Nb, (b) Ti–13Nb–13Zr and (c) Ti–15Zr–4Nb alloys.

Since the oxide layers have been produced to improve the behavior of these materials against corrosion, they must provide a better protection than the passive layer formed in air. For this goal the scales should be compact, adherent and thick enough to ensure the maximum protection. The oxide scale of the Ti–6Al–7Nb alloy represented in Fig. 1a was rather thin, and it was concluded that an increase of the scale thickness could be beneficial to ensure a better protection. Thus, for this alloy the oxidation time was increased to 48 h attempting to increase the oxide thickness. The cross-sectional view of the Ti–6Al–7Nb alloy oxidized for 48 h at 750 °C is shown in Fig. 2a. As it is observed in this micrograph, the scale formed with this new treatment time was quite similar to that formed after 24 h of oxidation, and only a slight thickness increase was detected. This result indicates that the oxidation rate for this alloy is very slow, which is probably related to the formation of a compact scale. This kind of scales usually has excellent protective properties.

In the case of the TiNbZr alloys, the scales represented in Fig. 1b and c have numerous pores and some longitudinal fissures at the metal-oxide interface. These cracks can produce a detachment of some regions of the scale and, therefore, a worse protection against corrosion. Spallation in other Ti alloys has been observed after the scale has reached a critical thickness. All these observations as well as the considerable thickness of the scales suggest a too long thermal treatment time. Therefore, the oxidation time for the TiNbZr alloys was diminished to 6 h trying to obtain a thinner layer and, thus, to avoid the longitudinal fissures. Fig. 2b and c exhibit the cross-sectional views of the Ti–13Nb–13–Zr and Ti–15Zr–4Nb alloys samples oxidized for 6 h at 750 °C. These micrographs show that the scales obtained with this new treatment time were thinner, around 3 and 10 μm for Ti–13Nb–13Zr and Ti–15Zr–4Nb, respectively. However, the new scales still presented some longitudinal fissures and their appearance was similar to that of the previous ones, with many pores.

Identification of the main phases forming the oxide layers was carried out using the XRD patterns obtained from the oxidized alloys. The sample depth of copper K_α radiation under the operation conditions is in the range from 10 to 20 μm. Therefore, in the case of scales which are thinner than the XRD sample depth, the XRD

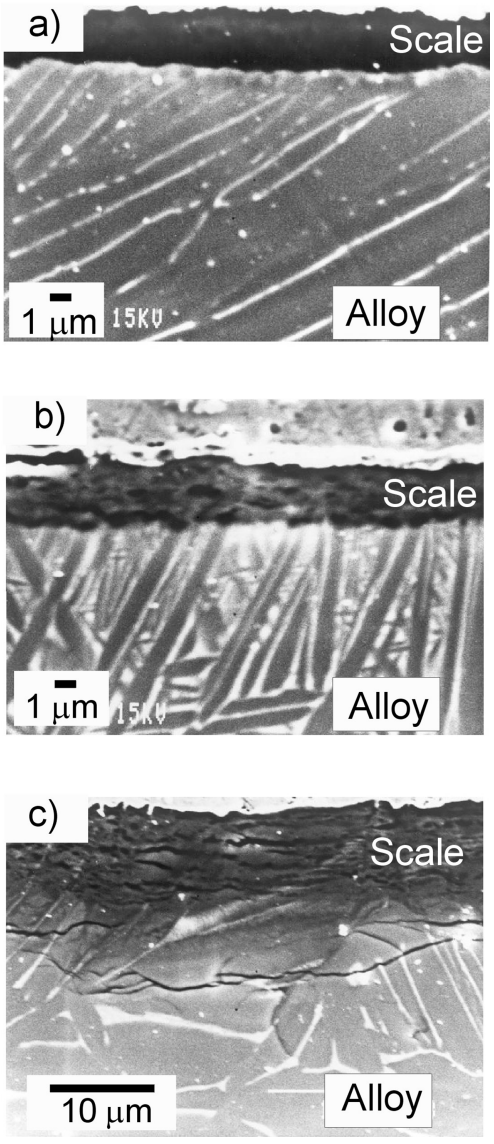

Fig. 2. Cross-sectional SEM micrograph of the oxide scale formed after an oxidation treatment at 750 °C a) for 48 h on Ti–6Al–7Nb, b) for 6 h on Ti–13Nb–13Zr and c) for 6 h on Ti–15Zr–4Nb alloys.

diagram will give also information of the metallic substrate. For the same alloy, the difference between XRD patterns for different oxidation times was the presence and intensity of the metallic emission. The longer the oxidation times the thicker the scale and the lower the metallic emission. Consequently, the XRD patterns that will provide more reliable information on the main phases forming the oxide layer are the corresponding to the thicker scales. Thus, Fig. 3 shows the XRD pattern of Ti–6Al–7Nb after a heat treatment at 750 °C during 48 h and of Ti–13Nb–13Zr and Ti–15Zr–4Nb after a heat treatment at 750 °C during 24 h. For the oxidized Ti–6Al–7Nb alloy, the XRD pattern shows the presence of three phases: TiO_2, Al_2O_3 and α-Ti, as can be observed in Fig. 3. Since in this case the sample depth is larger than the thickness of the oxide

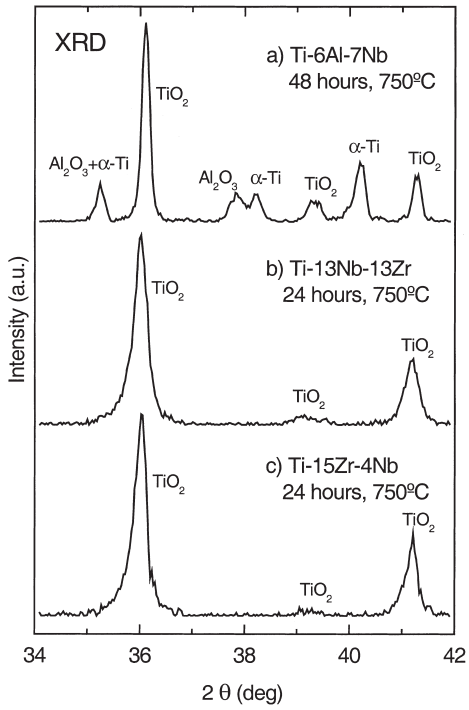

Fig. 3. XRD pattern after oxidation at 750 °C: (a) Ti–6Al–7Nb for 48 h (b) Ti–13Nb–13Zr for 24h and (c) Ti–15Zr–4Nb for 24 h.

scale, the α-Ti signal coming from the substrate was expected. On the other hand, the XRD patterns of the TiNbZr alloys oxidized at 750 °C for 24 h are formed mainly by TiO_2 rutile, as shown in Fig. 3. However, a small contribution of $TiZrO_4$ has been also detected at lower diffraction angles than those represented in Fig. 3. Comparing the three spectra of Fig. 3, it can be observed a small shift of the XRD's peaks corresponding to TiO_2 towards lower Bragg angles for the TiNbZr oxidized samples. This displacement was associated with an increase on the TiO_2 lattice parameter produced by the presence of Zr and Nb atoms.

The corrosion behavior of the oxidized alloys was evaluated by means of different electrochemical techniques. These tests were carried out to determine the protective capacity of the oxide layer formed on Ti–6Al–7Nb after a heat treatment at 750 °C during 48 h, and on the two TiNbZr alloys after a heat treatment at 750 °C during 6 h. These oxidation times were selected taking into account that the scales formed under these thermal conditions show the most favorable dimensions and appearances as protective layers. Hereafter, the three alloys after these thermal treatments will be called oxidized alloys.

Fig. 4 exhibits the corrosion current density values, i_{corr}, for the three oxidized alloys versus testing time. These data have been determined using the Stern–Geary equation [21] and taking into account the R_p values obtained by the linear polarization method. The values are in a band around 2×10^{-8} and 3×10^{-9} A cm^{-2}

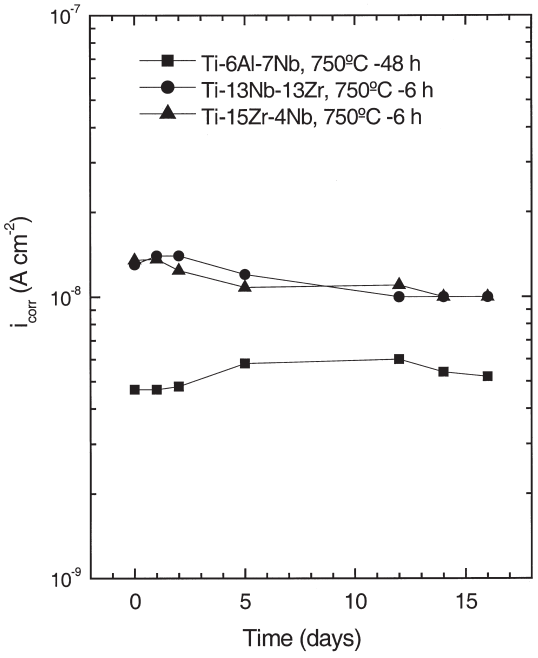

Fig. 4. Corrosion current densities, i_{corr}, vs. testing time for the three different oxidized Ti alloys in Hank's solution as calculated by using the polarization resistance method.

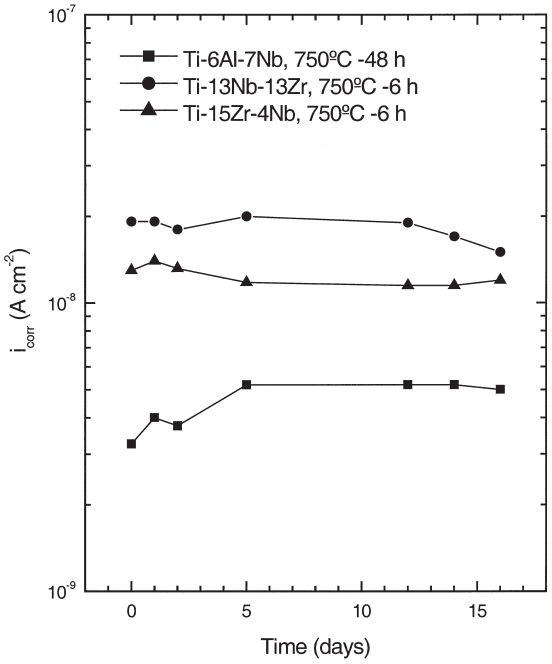

Fig. 5. Corrosion current densities, i_{corr}, vs. testing time for the three different oxidized Ti alloys in Hank's solution as deduced from the EIS.

with a rather stable behavior during the testing period. However, the Ti–6Al–7Nb oxidized alloy shows lower values than the TiNbZr alloys. This result indicates a better corrosion resistance for the Al-containing oxidized alloy. This effect was expected from the SEM investigation, since the Ti–6Al–7Nb oxidized alloy exhibited a more compact and dense oxide layer than the TiNbZr oxidized alloys.

The EIS was applied on the oxidized alloys to verify these corrosion results. The transfer resistance, R_T, estimated from the EIS measurements, is similar in some cases to the R_p determined by the direct current techniques. Therefore, taking into account the Stern–Geary equation and the R_T values, the corrosion current densities were calculated and are represented in Fig. 5 as a function of testing time for the three oxidized alloys. The i_{corr} values obtained by EIS are very similar to those calculated with the linear polarization data. Again, these values are very stable with the testing time. However, the corrosion current densities of the TiNbZr oxidized alloys do not show any improvement as compared with the data of the alloys without scale [20]. This result indicates that the oxide layer is a very porous film that allows the access of the electrolyte to the substrate. As a consequence, the corrosion behavior is similar to that of the as-received alloys. This agrees with the SEM observation of the TiNbZr oxidized alloys, where the observed scales appeared rather porous and with some fissures. For the Ti–6Al–7Nb oxidized alloy, the corrosion current density values are slightly better than that of this alloy without scale [20]. This result indicates that the oxide layer formed during the oxidation process on Ti–6Al–7Nb has a protective capacity.

In order to evaluate the susceptibility to pitting corrosion cyclic anodic polarization curves were measured on the oxidized alloys. Fig. 6 exhibits these curves

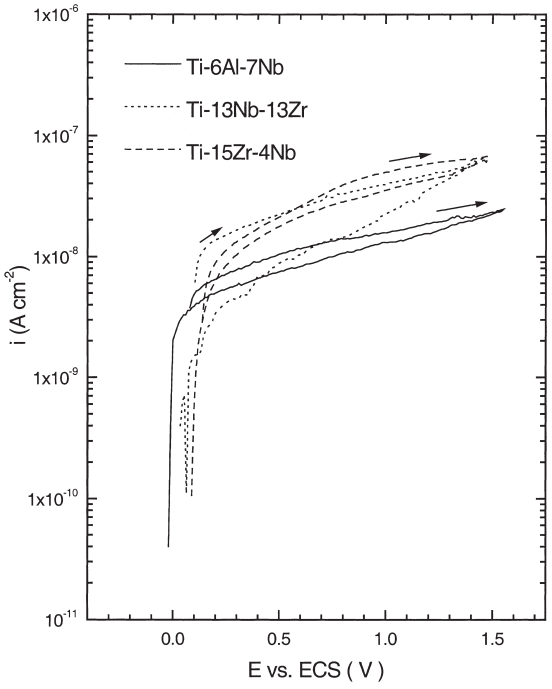

Fig. 6. Anodic polarization curves recorded at 10 mV min^{-1} for the three different oxidized Ti alloys after 18 days of immersion in Hank's solution.

Table 1
Fundamental parameters deduced from the cyclic anodic polarization curves corresponding to oxidized Ti–6Al–7Nb, Ti–13Nb–13Zr and Ti–15Zr–4Nb alloys

Material	E_{corr} (V)	I_p (A cm^{-2})
Ti–6Al–7Nb	0.08	1.0×10^{-8}–2×10^{-8}
Ti–13Nb–13Zr	0.104	1.5×10^{-8}–$5 \cdot 10^{-8}$
Ti–15Zr–4Nb	0.138	1.5×10^{-8}–$6 \cdot 10^{-8}$

for oxidized Ti–6Al–7Nb, Ti–13Nb–13Zr and Ti–15Zr–4Nb alloys after 18 days of immersion in Hank's solution. Table 1 represents the main parameters deduced from these anodic polarization curves, the corrosion potential, E_{corr}, and the passivation current density, i_p. The anodic polarization curves usually allow the determination of the breakdown potential, at which the outer layer breaks locally. At this point, a sudden increase of the current density is detected due to the scale crack. However, as already observed in previous works in titanium alloys immersed in Hank's solution [20,22], no breakdown is observed and the wide passivation region suggests that the material is in a passive stable state. This result indicates that the probability of pitting corrosion attack is very low for the three studied alloys. The current density values for the two TiNbZr oxidized alloys are very similar. However, the Ti–6Al–7Nb oxidized alloy shows the lowest current density, which indicates a better corrosion behavior in agreement with the results obtained for the uniform corrosion process. The comparison of the anodic polarization curves of Fig. 6 with those of the as-received alloys reveals lower current density values for the oxidized alloys [20]. Thus, a better pitting corrosion behavior is obtained for the three oxidized samples than for the non-oxidized alloys. This result suggests that for the three Ti alloys the oxidation process gives rise to the formation of an oxide layer that improves the protection against pitting attack. Moreover, the anodic polarization curves of the three oxidized alloys show current densities also lower than that found in the conventional biomaterial Ti–6Al–4V [22]. Other usual biomaterials such as Co alloys or coated stainless steels show similar current densities to that found in the oxidized Ti alloys but a breakdown potential is reached after 0.5 V of polarization [22]. This comparison indicates the excellent pitting corrosion behavior of the three oxidized alloys.

4. Conclusions

Three Ti alloys, Ti–6Al–7Nb, Ti–13Nb–13Zr and Ti–15Zr–4Nb, have been thermally treated with the aim of generating a protective oxide layer on their surface. The thickness of the layers formed at 750 °C during 24 h varies strongly depending of the alloy. The main phase observed in the oxide films of the TiNbZr treated alloys is TiO_2 rutile. However, in the case of the Ti–6Al–7Nb a contribution of Al_2O_3 is also detected.

The SEM images show a more dense oxide layer for the Ti–6Al–7Nb oxidized alloy. The two TiNbZr oxidized samples exhibited a porous layer with some small longitudinal fissures.

With the aim of improving the properties of the oxide layers, different heat treatment times were studied. After selecting for each alloy the most favorable thermal conditions, the corrosion behavior of the heat treated alloys immersed in Hank's solution was evaluated. Thus, Ti–6Al–7Nb oxidized at 750 °C during 48 h and Ti–13Nb–13Zr and Ti–15Zr–4Nb oxidized at 750 °C during 6 h were investigated by different electrochemical techniques.

The results showed that the Ti–6Al–7Nb alloy oxidized at 750 °C during 48 h exhibits the lowest corrosion rates. This result is related to the SEM observations, where a more dense oxide layer was detected for this oxidized alloy. This uniform corrosion behavior has been confirmed by both direct and alternate current electrochemical methods.

The oxidized Ti–6Al–7Nb alloy also shows the best pitting corrosion behavior. However, for all oxidized titanium alloys the probability of pitting formation is very low. A comparison with previous results obtained on non-oxidized alloys reveals a better pitting corrosion behavior for the oxidized alloys. Thus, the scales formed on the alloys after the thermal treatment improve the protection of the material against the pitting attack due to the aggressive environment.

In summary, the morphology of the scale formed on the oxidized Ti–6Al–Nb alloy together with its excellent corrosion behavior make this surface-modified alloy the best of the three studied materials for biomedical applications. On the other hand, although the corrosion behavior of the two oxidized TiNbZr alloys is satisfactory, both of them are unsuitable as biomaterials due to the longitudinal fissures observed in their metal–oxide interface.

Acknowledgements

The authors are gratefully acknowledged to Professor G. Fommeyer from Max Planck Institut für Eisenforschung (Düsseldorf) for kindly supplying the Ti alloys specimens. This work has been supported by the Project 07N-0050-1999 of the Spanish 'Programa de Tecnología de los Materiales de la Comunidad Autónoma de Madrid'. One of the authors (A.G.) thanks the Spanish Ministerio de Ciencia y Tecnología for financial support through the 'Ramón y Cajal' Programme.

References

[1] H. Sibum, V. Güther, O. Roidl, in: F. Habashi (Ed.), Alloys (Ch. 11), Wiley-VCH, Weinheim, 1998.
[2] R. Boyer, G. Welsch, E.E. Collings, Materials Properties Handbook: Titanium Alloys, ASM International, Materials Park, OH, 1994.
[3] R. Strietzel, A. Hosch, H. Kalbfleisch, D. Buch, Biomaterials 19 (1998) 1495.
[4] H.J. Breme, V. Biehl, J.A. Helsen, in: J.A. Helsen, H.J. Breme (Eds.), Metals as Biomaterials (Ch. 2), Wiley, Chichester, 1998.
[5] D.H. Kohn, P. Ducheyne, in: D.F. Williams (Ed.), Medical and Dental Materials. Serie Materials Science and Technology, vol. 14 (Ch. 2), VCH, Weinheim, 1992.
[6] M.F. Lopez, A. Gutiérrez, J.A. Jiménez, Surf. Sci. 482–485 (2001) 300.
[7] F.A. Akin, H. Zreiqat, S. Jordan, M.B.J. Wijesundara, L. Hanley, J. Biomed. Mater. Res. 57 (2001) 588.
[8] T. Sohmura, H. Tamasaki, T. Ohara, J. Takahashi, J. Biomed. Mater. Res. 58 (2001) 478.
[9] A.K. Lynn, D.L. DuQuesnay, Biomaterials 23 (2002) 1937.
[10] I.C. Lavos-Valetero, S. Wolynec, M.C.Z. Deboni, Jr., B. König, J. Biomed. Mater. Res. 58 (2001) 727.
[11] M.T. Pham, W. Matz, D. Grambole, F. Herrmann, H. Reuthe, E. Richter, G. Steiner, J. Biomed. Mater. Res. 59 (2002) 716.
[12] K. Kuroda, R. Ichino, M. Okido, O. Takai, J. Biomed. Mater. Res. 59 (2002) 390.
[13] T. Mano, Y. Ueyama, K. Ishikawa, T. Matsumura, K. Suzuki, Biomaterials 23 (2002) 1931.
[14] D. Velten, V. Biehl, F. Aubertin, B. Valeske, W. Possart, J. Breme, J. Biomed. Mater. Res. 59 (2002) 18.
[15] M.L. Escudero, J.L. González-Carrasco, C. García-Alonso, E. Ramírez, Biomaterials 16 (1995) 735.
[16] M.F. López, A. Gutiérrez, M.C. García-Alonso, M.L. Escudero, J. Mater. Res. 13 (1998) 3411.
[17] Y. Okazaki, S. Rao, Y. Ito, T. Tateishi, Biomaterials 19 (1998) 1197.
[18] M.A. Khan, R.L. Williams, D.F. Williams, Biomaterials 20 (1999) 631.
[19] M.A. Khan, R.L. Williams, D.F. Williams, Biomaterials 20 (1999) 765.
[20] M.F. López, A. Gutiérrez, J.A. Jiménez, Electrochim. Acta 47 (2002) 1359.
[21] M. Stern, A.L. Geary, J. Electrochem. Soc. 104 (1957) 56.
[22] M.L. Escudero, M.F. López, J. Ruiz, M.C. García-Alonso, H. Canahua, J. Biomed. Mater. Res. 31 (1996) 313.